Solar Energy 186 (2019) 392–397

Contents lists available at ScienceDirect

Solar Energy

journal homepage: www.elsevier.com/locate/solener

Optical properties of a random inverted pyramid textured silicon surface studied by the ray tracing method

Quansheng Chen[a,c], Yaoping Liu[a,b,*], Yan Wang[a,b], Wei Chen[a,b], Juntao Wu[a,c], Yan Zhao[a,c], Xiaolong Du[a,b,c,*]

[a] Key Laboratory for Renewable Energy, Beijing Key Laboratory for New Energy Materials and Devices, Beijing National Laboratory for Condensed Matter Physics, Institute of Physics, Chinese Academy of Sciences, Beijing 100190, China
[b] Songshan Lake Materials Laboratory, Dongguan, Guangdong 523808, China
[c] School of Physical Sciences, University of Chinese Academy of Sciences, Beijing 100049, China

ARTICLE INFO

Keywords:
Silicon solar cells
Random inverted pyramid
Texture
Ray tracing

ABSTRACT

The random inverted pyramid texture has been extensively studied experimentally in high-efficiency monocrystalline silicon solar cells due to its superior optical properties. In this paper, a random inverted pyramid structure model was established, and the optical performance was studied by the ray tracing method. It has five common light paths and can achieve lower reflectance than random upright pyramids. To further analyze the optical properties of random inverted pyramids, a simplified random inverted pyramid model, which consists of two overlapping inverted pyramids, was studied and analyzed in detail. The proportions of the light path related to different overlapping regions, and the reflectance ranging from 10.11% to 10.64%, can be obtained, which is lower than the reflectivity of random upright pyramids. We believe that the random inverted pyramid texture can have a wide range of applications in high-efficiency monocrystalline silicon solar cells.

1. Introduction

Efficient light absorption is a key technology for improving the efficiency of solar cells. Surface texture is a common way to improve light absorption and reduce reflections for silicon solar cells by light trapping (Polman et al., 2016; Razykov et al., 2011). Many surface-modified structures have been extensively studied experimentally and theoretically, such as upright pyramids (UPs) (Moreno et al., 2014; Zhong et al., 2016; Baker-Finch and McIntosh, 2013), inverted pyramids (IPs) (Wang et al., 2015; Zhao et al., 1995; Smith and Rohatgi, 1993); nanopores (Yuan et al., 2009), worm-like pits (González-Díaz et al., 2009), and V-shaped textures (Untila et al., 2013).

Among them, the upright pyramid structure is widely used in monocrystalline silicon solar cells, which are produced by etching (1 0 0)-oriented monocrystalline wafers in an alkaline solution such as NaOH or KOH (Moreno et al., 2014). The optical performance of the upright pyramid is theoretically analyzed and studied based on the ray tracing method (Baker-Finch and McIntosh, 2011; Campbell and Green, 1987; Yagi et al., 2006; Magnin et al., 2014).

The ray tracing method is a relatively common method that can be used to calculate the ray path and optical properties of structures. By using a planar silicon model and a planar silicon model covered with glass, the ray tracing simulation is evaluated to be very effective and reliable. The optical properties of several thin-film silicon cells with V-groove structures were analyzed by this method (Yagi et al., 2006). Both regular upright pyramids and inverted ones were investigated, and the directional-hemispherical reflectance was calculated under different azimuth and incidence angles by the ray tracing method (Magnin et al., 2014).

Based on the previous study, the optical properties of the regular inverted pyramid structure are believed to be superior to those of the upright pyramid structure. The regular inverted pyramid structures, which are prepared by photolithography, can experimentally produce a highly efficient silicon solar cell (Zhao et al., 1998). However, the expensive fabrication cost limits the application in the solar cell industry. The wet etching method for the fabrication of inverted pyramids has been extensively studied in recent years. One way is to fabricate a micron-sized inverted pyramid structure by copper-catalyzed chemical etching (Baker-Finch and McIntosh, 2013; Li et al., 2017; Treideris et al., 2018). Another way is to postmodify a nanowire or nanopore structure using an alkaline solution so that a nanomicron inverted pyramid structure can be fabricated (Jiang et al., 2017). Hence, only a

* Corresponding authors at: Key Laboratory for Renewable Energy, Beijing Key Laboratory for New Energy Materials and Devices, National Laboratory for Condensed Matter Physics, Institute of Physics, Chinese Academy of Sciences, Beijing 100190, China (X. Du).
E-mail addresses: ypliu@iphy.ac.cn (Y. Liu), xldu@iphy.ac.cn (X. Du).

https://doi.org/10.1016/j.solener.2019.05.031
Received 11 January 2019; Received in revised form 8 May 2019; Accepted 13 May 2019

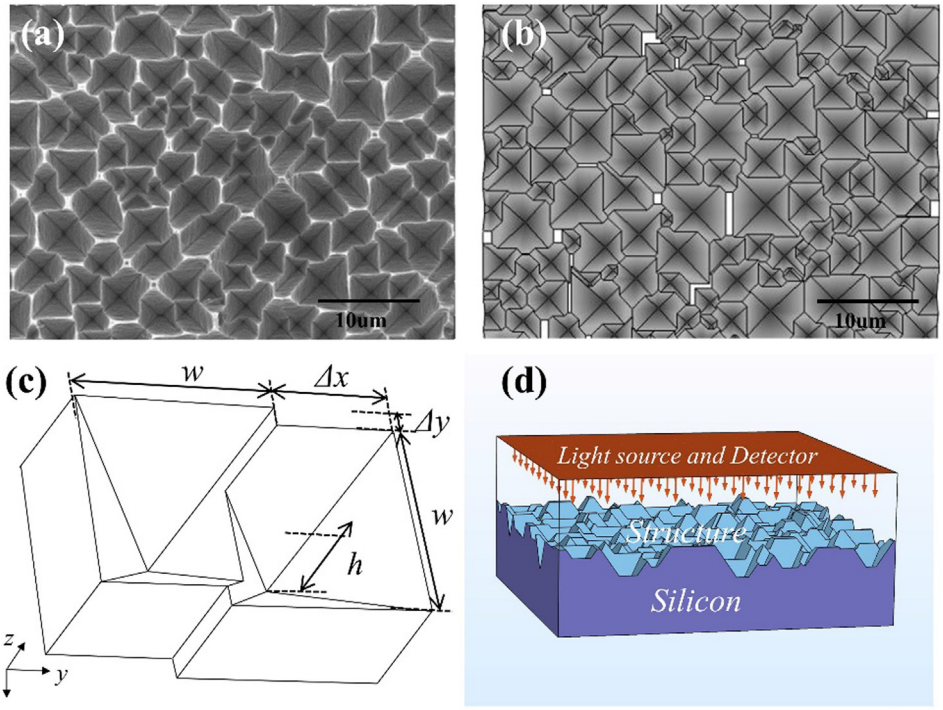

Fig. 1. (a) SEM top-view image of the random inverted pyramid. (b) Mathematical model of the random inverted pyramid. (c) Schematic of the overlap inverted pyramid structure model. (d) Schematic of the ray tracing simulation model.

random inverted pyramid structure can be formed on the surface of the silicon wafer by two maskless techniques. However, there are few reports including detailed analysis of the optical properties of random inverted pyramids.

In this paper, a random inverted pyramid texture model was established based on the experimental results, while the optical performance was analyzed based on the ray tracing method. We found that the proportion of random inverted pyramids light paths is quite different from that of random upright pyramids, and random inverted pyramids can achieve lower reflectance than random upright pyramids. To further study the random inverted pyramid texture, we designed an overlapping inverted pyramid model as a simplified random inverted pyramid model and analyzed the optical performance of this model. The proportions of the light paths were calculated in different overlapping regions, and the reflectivity was obtained under different overlapping conditions.

2. Model and simulation

As shown in Fig. 1(a), a micron-scale inverted pyramid structure is fabricated on the surface of the silicon wafer by a one-step maskless copper catalytic chemical etching method, and the specific experimental parameters can be found in previous papers (Wang et al., 2015). The size of the random inverted pyramids ranges from 2 to 6 μm. The mathematical random inverted pyramid textures are established by computer-generated random numbers, as shown in Fig. 1(b). The position of the inverted pyramid randomly appears in the restricted area, and the size of the inverted pyramid ranges from 2 to 6 μm. The appropriate number of inverted pyramids is used for covering the silicon surface according to experimental results. We find that the random inverted pyramid texture is similar between Fig. 1(a) and (b). Several inverted pyramids overlap, and there is a very small platform in the texture.

To further explain the optical performance of the random inverted pyramid, we propose a simplified model consisting of two overlapping inverted pyramid structures, as shown in Fig. 1(c). The width of the inverted pyramid is w and the depth is h. Based on the anisotropic etching mechanism of Cu^{2+}, the inverted pyramid formed by the {1 1 1} crystal plane is formed on the surface of the (1 0 0)-oriented silicon wafer, so $h = w/\sqrt{2}$ (Chen et al., 2018). Δx and Δy represent the offset distances in the x and y directions between the two inverted pyramids, respectively. When the width, w, changes, the proportion of the ray path does not change (Yang et al., 2016), so the width, w, of the structure does not affect the result. In this paper, w is selected to be 5 μm

Compared with the Finite-Difference Time-Domain (FDTD) method based on Maxwell's equations (Zhong et al., 2016), ray tracing ignores the effect of the wave theory of light on optical performance. Hence, the division of the grid can be larger than the wavelength scale. In addition, the optical simulation calculations can be performed for the structures larger than the micrometer scale. As shown in Fig. 1(d), the plane above the structure is set as an incident light source. The light is perpendicularly irradiated onto the surface of the silicon wafer, which has a microstructure on the surface. Moreover, the plane is also a collecting detector for reflecting light energy, and all the light energy after the interaction with the structure is collected in this plane. To collect all of the reflected energy completely, the area of the plane needs to be large enough, so the size of the collecting detector is larger than the size of the incident light source. In the two-dimensional model, when the number of incident rays is 200, the relative error between adjacent rays is only 0.5%, which can meet the needs of the study completely (Yang et al., 2016). Hence, considering the three-dimensional model and computer performance, each model uses as much light as possible for each calculation; the number of rays is 100,000, which were randomly generated with a total power of 1 W. The material of the substrate is silicon, and its characteristic refractive index is a function of wavelength. The remaining boundary condition is the 'pass through' condition, which means that all light energy is absorbed in the silicon material. It means that we ignore the reflections of longer infrared wavelengths on the backside of the wafer.

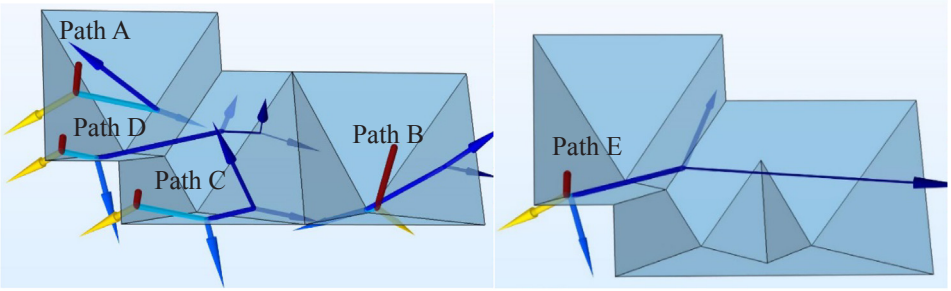

Fig. 2. Schematic of Paths A, B, C, D and E. The color and width of the ray paths represent the energy of the light.

3. Result and analysis

Light propagates to the interface between air and silicon, producing a reflected light and a refracted light based on the law of reflection. The refracted light enters the silicon material, and then the energy of the refracted light is absorbed by the silicon and produces photogenerated carriers. The reflected light will continue to propagate in the air. Some of this reflected light may undergo the reflection and refraction at the next interface until all of the reflected light escapes from the silicon surface into the air. The ratio between the light energy going back to the air and incident light energy is defined as reflectivity. The reflectivity is determined by the structure and materials. We can obtain the reflectivity by analyzing the propagation path of each incident ray in different structures.

In the regular inverted pyramid, there are three ray paths, as shown in Fig. 2: Paths A, B, and C (Baker-Finch and McIntosh, 2011). Path A experiences a double bounce on the silicon surface, and Paths B and C undergo a triple bounce. The color and width of the ray paths represent the energy of the light. Paths A, B, and C complete all propagation paths in a single inverted pyramid. However, as shown in Fig. 1(a), when there are multiple inverted pyramids overlapping, as the structure becomes more complicated, the incident light may propagate in multiple inverted pyramids, so there will be quadruple or more bounces. As shown in Fig. 2, some rays defined as Path D undergo a quadruple bounce, which only exists in not less than two overlapping inverted pyramids. In a random inverted pyramid structure, there are at most seven ray paths, which are the same as for random upright pyramids. In addition to the above four ray paths, there is also a triple bounce, as shown in Fig. 2 and defined as Path E. Path E exits only in three or more than three overlapping inverted pyramids. The probability of the existence of the other two ray paths is extremely low, so they will not be discussed in this letter.

The relationship between the total reflectivity, $R_{i,\lambda}$(i = A, B, C, D, E), of each ray path with wavelength is shown in Fig. 3. The weighted average reflectance, R_i(i = A, B, C, D, E), is defined as follows:

$$R_i = \frac{\int_{300}^{1000} N(\lambda) R_{i,\lambda} d\lambda}{\int_{300}^{1000} N(\lambda) d\lambda} \quad (1)$$

where $R_{i,\lambda}$ is the total reflectance at the wavelength of λ, and $N(\lambda)$ is the solar flux under AM 1.5 standard conditions (Menna et al., 1995). Path A has only two chances for interacting with the silicon surface, so the reflectivity is the largest and the light absorption is minimal. The weighted average reflectance is R_A = 13.85%. Paths B, C and E have three chances for interacting on the silicon surface, but the reflectance is quite different. Path B has the highest reflectance, while Path E has the lowest. The weighted average reflectance values are R_B = 11.02%, R_C = 5.23% and R_E = 1.02%. Two reasons can explain the phenomenon. One is that the angle of incidence at the third bounce along Path B is large (θ_3 = 86.32°) so that almost all light is reflected, as shown in Fig. 2. The other reason is that most of the *p*-polarization light is absorbed at the second bounce for Paths C and E, and then the remaining *s*-polarized light is converted to *p*-polarization before starting the third reflection for only Path E. Hence, the reflectance of Path E becomes very low after the converted *p*-polarization light is almost all absorbed at the third bounce. The incidence angle of the second and third bounce is close to Brewster's angle. Path D experiences a quadruple bounce, one more bounce than Path E, so it can achieve a lower reflectance than Path E. The weighted average reflectance, R_D, is 0.56%. Path D requires the existence of an adjacent inverted pyramid and propagates into the adjacent inverted pyramid after the second bounce.

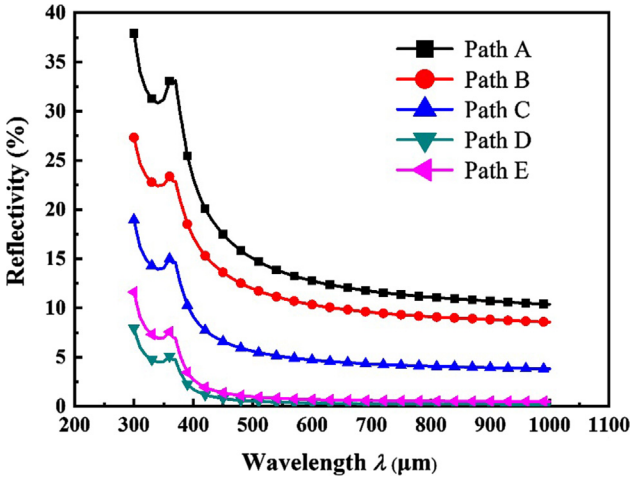

Fig. 3. Reflectivity spectra in different ray paths.

The three kinds of silicon surfaces, regular upright pyramid, regular inverted pyramid and random upright pyramid, have different proportions of light paths f_i (i = A, B, C, D, E), as previously reported (Baker-Finch and McIntosh, 2011; Yang et al., 2017). As shown in Table 1, the regular pyramid structure has a very high proportion of Path A, f_A = 88.89%, and the remainder is Path B, f_B = 11.11%. The regular inverted pyramid has a new light path, Path C, and it has a higher proportion, f_C = 40%. Hence, the proportion of Path A reduces greatly; f_A = 59.26%. Path B has a very low proportion, f_B = 0.74%, due to existing only at the bottom of the inverted pyramid. The light paths in the regular upright and inverted pyramid are easy to study, and the proportion of light paths is a determined result. However, the two distinct models for random upright pyramids can provide different results regarding the proportion of light paths. There are seven light paths

Table 1
The proportions, f_i, of four ray paths and the weighted average reflectance values, $R_{structure}$, in a regular/random UP and regular IP structure.

	Path A	Path B	Path C	Path D	Path E	$R_{structure}$
Regular UP	88.89%	11.11%	0	0	0	13.54%
Random UP	68.33%	3.24%	18.6%	5.83%	3.74%	10.86%
Regular IP	59.26%	0.74%	40%	0	0	10.38%
Random IP	61.29%	0.21%	37.52%	0.46%	0.52%	10.48%

in the random upright pyramid structure, and we neglect to discuss two of them because their probability is extremely low. The proportion of Path A in the random upright pyramid is significantly decreased compared to the regular upright pyramid, $f_A = 68.33\%$, but is still higher than that of the regular inverted pyramid. A proportion of Path C appears in the random upright pyramid, $f_C = 18.6\%$, but the proportion is lower than that of the regular inverted pyramid. Path D and Path E have some proportions in random upright pyramids, with $f_D = 5.83\%$ and $f_E = 3.74\%$.

The ray tracing simulation calculation is used for mathematical random inverted pyramids, as shown in Fig. 1(b). Note that in both cases, the impact of the flat area on the results is not considered. The result of the calculation is related to the randomly generated structure, which is the same as the random upright pyramid, so the average proportion of ray paths can be obtained by multiple calculations. The proportions of different ray paths are $f_A = 61.29\%$, $f_B = 0.21\%$, $f_C = 37.52\%$, $f_D = 0.46\%$ and $f_E = 0.52\%$. The random inverted pyramid has a lower proportion of Path A and a higher proportion of Path C than the random upright pyramid. The proportions of Path D and Path E are all lower than the random upright pyramid because rays are less likely to propagate into adjacent structures than in upright pyramids.

The weighted average reflectance $R_{structure}$ of the surface of the silicon material can be calculated according to the following Eq. (2):

$$R_{structure} = f_A R_A + f_B R_B + f_C R_C + f_D R_D + f_E R_E \quad (2)$$

where R_A, R_B, R_C, R_D and R_E are the weighted average reflectance values of Paths A, B, C, D and E. f_A, f_B, f_C, f_D and f_E are the proportions of Paths A, B, C, D and E. The regular upright pyramid has the highest reflectivity, and the weighted average reflectance of a regular upright pyramid, $R_{regular\ UP}$, is 13.54%. The reflectivity of the random upright pyramid is second, and the weighted average reflectance of the random upright pyramid, $R_{random\ UP}$, is 10.86%. The regular inverted pyramid can exhibit the lowest reflectivity, and the weighted average reflectance of a regular inverted pyramid, $R_{regular\ IP}$, is 10.38%. The weighted average reflectance of a random inverted pyramid can be obtained as $R_{random\ IP} = 10.48\%$. The high proportion of Path A results in the highest reflectivity for a regular upright pyramid. The proportion of Path A is still higher for the regular inverted pyramid than for the random upright pyramid structure, even if there are quadruple or more bounces. Hence, the regular inverted pyramid has the lowest reflectivity due to the lowest number of double bounces and the highest number of triple bounces. The reflectivity of the random inverted pyramid is slightly higher than that of the regular inverted pyramid due to the increase of the proportion of Path A and the decrease of the proportion of Path C.

To further study the random inverted pyramid structure, we design an overlapping inverted pyramid structure model, as shown in Fig. 1(c), and analyze the proportion of each ray path based on the ray tracing method, as shown in Fig. 4. Due to the symmetry of the structure, only the case where $\Delta x/w$ is greater than or equal to $\Delta y/w$ is analyzed. In Fig. 4(a), when $\Delta x/w = 0.6$ and $\Delta y/w = 0$, the proportion of Path A reaches a maximum of 62.22%, which is still lower than the random upright pyramids. In the four cases of ($\Delta x/w = 0.6$, $\Delta y/w = 0$), ($\Delta x/w = 0.5$, $\Delta y/w = 0$), ($\Delta x/w = 0.7$, $\Delta y/w = 0$) and ($\Delta x/w = 0.6$, $\Delta y/w = 0.1$), the distribution of the ray paths is shown in Fig. 5. When $\Delta y/w = 0$, the two inverted pyramids overlap only in the x direction. When $\Delta x/w$ increases from 0.6 to 0.7, the change in the proportion of Path C is larger than the change in the proportion of Path A for the increased region. Therefore, the proportion of Path A decreases, and the proportion of Path C increases, as shown in Fig. 5(c) (the red dotted frame shows the new region). When $\Delta x/w$ decreases from 0.6 to 0.5, the second bounce area of Path C increases, and the new region on both sides of the overlapping inverted pyramid structure experiences three bounces because the length of the sidewall along the x direction is larger than that of the regular inverted pyramid, as shown in Fig. 5(a) (the new increased region of the triple bounce is marked by the solid red circle). Therefore, the proportion of Path A decreases, and the proportion of Path C increases. When $\Delta x/w = 0.6$ and $\Delta y/w$ gradually increases from 0 to 0.1, the total area of the two overlapping inverted pyramid structure increases. The increased area almost always undergoes a triple bounce, so the proportion of Path A decreases and the proportion of Path C increases. When $\Delta y/w$ further increases, the total area of the overlapping inverted pyramid structure continues to increase, but the part of the three reflections no longer increases, which increases the part of the double bounce in turn. Therefore, when $\Delta x/w = 0.6$ and $\Delta y/w = 0.6$, the proportion of Path A achieves a maximum value with a proportion of 61.68%. When $\Delta x/w = 0.2$ and $\Delta y/w = 0.2$, the proportion of Path A reaches a minimum value of 57.37%.

Path B appears in a small area of the inverted pyramid apex, resulting in a low proportion of Path B, as shown in Fig. 4(b). Therefore, the change in the sum of the proportions of Path C and Path D is completely opposite the change in the proportion of Path A. Fig. 4(c) shows the proportion of Path C. The proportion of Path C reaches its lowest value of 35.38% at $\Delta x/w = 0.6$ and $\Delta y/w = 0.6$ and reaches a local minimum of 37.00% at $\Delta x/w = 0.6$ and $\Delta y/w = 0$. The change in Path C is almost the opposite the change in Path D because the region of Path D is transformed on the basis of Path C. Only when $\Delta x/w$ is approximately 0.45 and $\Delta y/w$ is approximately 0.45 does the proportion of Path D exceed 3%. However, for other cases, the proportion of Path C is approximately 40.1%, and the proportion of Path D is approximately 0.

The result of the ray paths is independent of the incident wavelength based on the ray tracing method. Fig. 6 shows the weighted average reflectance of overlapping inverted pyramid structures with different values of $\Delta x/w$ and $\Delta y/w$. When $\Delta x/w = 0.6$ and $\Delta y/w = 0$, the maximum reflectance reaches 10.64%. When $\Delta x/w = 0.6$ and $\Delta y/w = 0.6$, the reflectance reaches a maximum value of 10.56%. When $\Delta x/w = 0.3$ and $\Delta y/w = 0.3$, the reflectance reaches a minimum of 10.11%. The reflectance of the overlapping inverted pyramid is comparable to that of a regular/random inverted pyramid. Path A has the largest reflectivity and dominates the overall structure reflectivity, so the change in the proportion of Path A is almost the same as the change in reflectance according to Figs. 4a and 6. Only when $\Delta x/w$ is approximately 0.45 and $\Delta y/w$ is approximately 0.45 does the proportion of Path D increase, resulting in the same low reflectivity in this area. Therefore, this can indicate that effectively increasing the proportion of Path D can reduce the reflectivity of the overlapping inverted pyramids if the proportion of Path A does not change much.

All overlapping possibilities in the inverted pyramid structures were analyzed, and the result suggests that the proportion of paths is related to the overlapping area. So, for different overlapping regions, the result of random inverted pyramid structures can be affected greatly, but the proportion of light paths and reflectance values still remain in a certain range. We notice that the results for the random inverted pyramid also meet the calculated result range of overlapping inverted pyramids, except that Path E only exists in the random inverted pyramid because the appearance of Path E requires more inverted pyramids to overlap.

We find that the simulation result of reflectance, whether under the random inverted pyramid model or the simplified overlapping inverted pyramid model, is higher than the experimental result, which was reported previously (Wang et al., 2015). The simulation result of reflectance only can obtain ~10.4%, but the experimental result can be as low as 5%. The reasons for this large difference between the two results may be as follows: first, the theoretically calculated structural surface is perfectly smooth, but the actual experimental structural surface has many nanostructures, resulting in lower reflectance. Moreover, the original silicon surface used in the experiment is uneven. Therefore, the inverted pyramid structures may have a large difference along the z-axis, and the difference along the z-axis may cause a further decrease in the reflectance of the silicon surface. In this paper, the top planes of all inverted pyramids are built on the same horizontal plane,

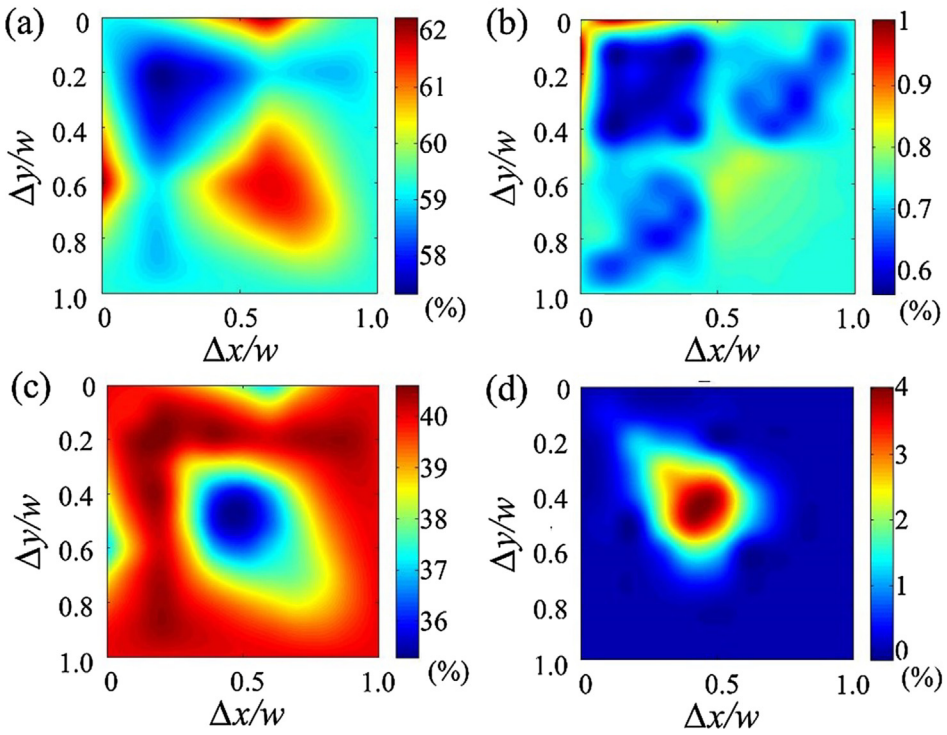

Fig. 4. The proportions of different ray paths in different overlapping areas. (a) Path A, (b) Path B, (c) Path C, and (d) Path D.

but the actually formed inverted pyramids still differ in the z-axis due to the mutual overlap between the inverted pyramids. The difference along the z-axis is limited by the size of the inverted pyramid, with a maximum difference of 2.83 um. Further increasing the difference along the z-axis is likely to reduce the reflectivity of the silicon surface.

4. Conclusion

In summary, the optical properties of random inverted pyramid structures were studied by the ray tracing method. This structure has five common ray paths and can obtain lower reflectivity than random upright pyramids, which are currently used in mass production. To further study the random inverted pyramid structure, the proposed overlapping inverted pyramid structure model was analyzed and studied. The proportion of the light paths is related to the overlapping regions, and reflectance values between 10.11% and 10.64% can be obtained, which is lower than the reflectivity of the random upright pyramid. Therefore, we believe the random pyramid structure has a greater application prospect in the field of monocrystalline silicon solar cells if it has an acceptable manufacturing cost.

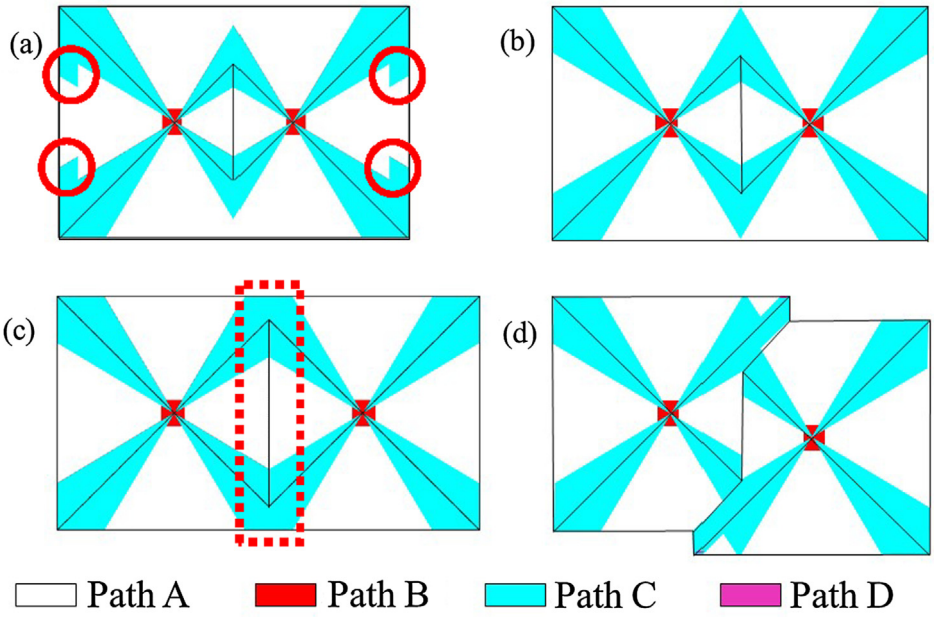

Fig. 5. Schematic of ray path distributions in the case of four overlapping inverted pyramids. (a) $\Delta x/w = 0.5$, $\Delta y/w = 0$, (b) $\Delta x/w = 0.6$, $\Delta y/w = 0$, (c) $\Delta x/w = 0.7$, $\Delta y/w = 0$, (d) $\Delta x/w = 0.6$, $\Delta y/w = 0.1$.

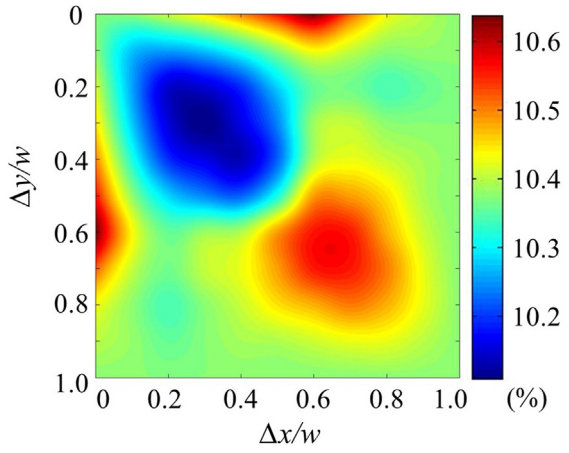

Fig. 6. The weighted average reflectance values for different overlapping inverted pyramid structures with different $\Delta x/w$ and $\Delta y/w$ overlaps.

Acknowledgements

This work was supported by the National Natural Science Foundation of China (Grant Nos. 11675280 and 11674405) and the Science and Technology Department of Jiangsu Province (Technological Achievements Transformation Project, Grant Nos. BA2017137). Thanks are due to Mr. Yueke Wang from the School of Science, Jiangnan University, for making some suggestions about this paper.

References

Baker-Finch, S.C., McIntosh, K.R., 2011. Reflection of normally incident light from silicon solar cells with pyramidal texture. Progress Photovol.: Res. Appl. 19 (4), 406–416.
Baker-Finch, S.C., McIntosh, K.R., 2013. Reflection distributions of textured monocrystalline silicon: implications for silicon solar cells. Progress Photovol.: Res. Appl. 21 (5), 960–971.
Campbell, P., Green, M.A., 1987. Light trapping properties of pyramidally textured surfaces. J. Appl. Phys. 62 (1), 243–249.
Chen, W., Liu, Y., Yang, L., et al., 2018. Difference in anisotropic etching characteristics of alkaline and copper based acid solutions for single-crystalline Si. Sci. Rep. 8 (1), 3408.
González-Díaz, B., Guerrero-Lemus, R., Díaz-Herrera, B., et al., 2009. Optimization of roughness, reflectance and photoluminescence for acid textured mc-Si solar cells etched at different HF/HNO_3 concentrations. Mater. Sci. Eng., B 159, 295–298.
Jiang, Y., Shen, H., Pu, T., et al., 2017. High efficiency multi-crystalline silicon solar cell with inverted pyramid nanostructure. Sol. Energy 142, 91–96.
Li, J.Y., Hung, C.H., Chen, C.Y., 2017. Hybrid black silicon solar cells textured with the interplay of copper-induced galvanic displacement. Sci. Rep. 7 (1), 17177.
Magnin, V., Harari, J., Halbwax, M., et al., 2014. Angle-dependent ray tracing simulations of reflections on pyramidal textures for silicon solar cells. Sol. Energy 110, 378–385.
Menna, P., Di Francia, G., La Ferrara, V., 1995. Porous silicon in solar cells: a review and a description of its application as an AR coating. Sol. Energy Mater. Sol. Cells 37 (1), 13–24.
Moreno, M., Murias, D., Martínez, J., et al., 2014. A comparative study of wet and dry texturing processes of c-Si wafers for the fabrication of solar cells. Sol. Energy 101, 182–191.
Polman, A., Knight, M., Garnett, E.C., et al., 2016. Photovoltaic materials: Present efficiencies and future challenges. Science 352 (6283), aad4424.
Razykov, T.M., Ferekides, C.S., Morel, D., et al., 2011. Solar photovoltaic electricity: Current status and future prospects. Sol. Energy 85 (8), 1580–1608.
Smith, A.W., Rohatgi, A., 1993. Ray tracing analysis of the inverted pyramid texturing geometry for high efficiency silicon solar cells. Sol. Energy Mater. Sol. Cells 29 (1), 37–49.
Treideris, M., Rėza, A., Kamarauskas, M., et al., 2018. Minimization of optical reflectance by copper assisted etching of crystalline silicon surface. Phys. Status Solidi (a) 215 (6), 1700600.
Untila, G., Palov, A., Kost, T., et al., 2013. Crystalline silicon solar cells with laser ablated penetrating V-grooves: Modeling and experiment. Phys. Status Solidi (a) 210 (4), 760–766.
Wang, Y., Yang, L., Liu, Y., et al., 2015. Maskless inverted pyramid texturization of silicon. Sci. Rep. 5, 10843.
Yagi, T., Uraoka, Y., Fuyuki, T., 2006. Ray-trace simulation of light trapping in silicon solar cell with texture structures. Sol. Energy Mater. Sol. Cells 90 (16), 2647–2656.
Yang, S., Ge, P., Zhang, L., 2016. The effects of different parameters of pyramidal textured silicon surface on the optical reflectance. Sol. Energy 134, 392–398.
Yang, L., Liu, Y., Wang, Y., et al., 2017. 18.87%-efficient inverted pyramid structured silicon solar cell by one-step Cu-assisted texturization technique. Sol. Energy Mater. Sol. Cells 166, 121–126.
Yuan, H.C., Yost, V.E., Page, M.R., et al., 2009. Efficient black silicon solar cell with a density-graded nanoporous surface: Optical properties, performance limitations, and design rules. Appl. Phys. Lett. 95 (12), 123501.
Zhao, J., Wang, A., Altermatt, P., et al., 1995. Twenty-four percent efficient silicon solar cells with double layer antireflection coatings and reduced resistance loss. Appl. Phys. Lett. 66 (26), 3636–3638.
Zhao, J., Wang, A., Green, M.A., et al., 1998. 19.8% efficient “honeycomb” textured multicrystalline and 24.4% monocrystalline silicon solar cells. Appl. Phys. Lett. 73 (14), 1991–1993.
Zhong, S., Wang, W., Zhuang, Y., et al., 2016. All-solution-processed random Si nanopyramids for excellent light trapping in ultrathin solar cells. Adv. Funct. Mater. 26 (26), 4768–4777.